

Evaluation of the Virtual Crystal Approximation for Predicting Thermal Conductivity

Jason M. Larkin¹ and A. J. H. McGaughey^{2,*}

¹*Department of Mechanical Engineering
Carnegie Mellon University
Pittsburgh, PA 15213*

²*Department of Mechanical Engineering
Carnegie Mellon University
Pittsburgh, PA 15213*

(Dated: December 15, 2012)

In this work, the virtual crystal approximation for mass disorder is evaluated by examining two model alloy systems: Lennard-Jones argon and Stillinger-Weber silicon. In both cases the perfect crystal is alloyed with a heavier mass species up to equal concentration and phonon properties and thermal conductivity are precited. These two alloyed systems have different ranges of phonon frequencies, lifetimes, and mean free paths. For Stillinger-Weber silicon, the virtual crystal approximation predicts phonon properties and thermal conductivity in good agreement with molecular dynamics-based methods. For Lennard-Jones argon, the virtual crystal approximation underpredicts the high frequency phonon lifetimes, leading to an underpredicting of its thermal conductivity. Resolution of these underpredictions is achieved by considering methods which treat the disorder explicitly.

I. INTRODUCTION

Accurately predicting the thermal conductivity of a dielectric or semiconducting material requires the properties of phonons from the entire Brillouin zone. Accurate predictions of phonon properties for bulk systems can be made with anharmonic lattice dynamics theory using ab initio calculations.^{1–8} However, computational costs limit the size of computational cells in ab initio calculations to be less than 100 atoms, making it difficult to directly incorporate the effects of disorder.^{4,5,7,9,10} Alternatively, theory that treats disorder as a harmonic perturbation can be used to estimate the reduction in phonon lifetimes due to disorder scattering without the use of a large unit cell.^{4,5,7} Under this approximation, the disordered crystal is replaced with a perfect virtual crystal with properties equivalent to an averaging over the disorder (e.g. mass or bond strength).¹¹

Recently, work using ab-initio calculations, anharmonic lattice dynamics (ALD) and the virtual crystal (VC) approximation was used to predict phonon mode frequencies, lifetimes and group velocities of materials with relatively large,^{4,5} moderate,⁷, and small⁷ thermal conductivities. The use of ALD and VC (referred to as VC-ALD) treats the effects of intrinsic and disorder scattering as perturbations rather than including disorder explicitly.(cite) However, no comprehensive study has been performed to assess the applicability of this perturbative approach for a range of heavily disordered systems using multiple predictive methods.

In intro, mention taud model, VC vs. Gamma point, NMD technique.

The goal of this work is to verify the use of the VC approximation for predicting thermal conductivity by a detailed comparison of 3 predictive methods: MD-based normal mode decomposition (NMD) and green-kubo (GK), and VC-ALD which treats the harmonic and

anharmonic phonon scattering as perturbations (Section II E 2). When used with the VC approximation, methods are referred to as VC-NMD and VC-ALD. Two model binary-alloy systems with varying concentrations (c) of mass defects ($m_{1-c}^a m_c^b$) are considered: Lennard-Jones (LJ) argon and Stillinger-Weber (SW) silicon. In both cases the perfect crystal is alloyed with a heavier mass species up to equal concentration, spanning a range of perturbative to heavy disorder. These two alloyed systems have very different ranges of phonon frequencies, lifetimes, group velocities and total thermal conductivity. For SW silicon, VC-ALD predicts thermal conductivity in good agreement with GK. For LJ argon, the VC-ALD approximation underpredicts the high frequency phonon lifetimes, leading to an underpredicting of the thermal conductivity. The different thermal conductivity spectra of and the breakdown of the perturbative models are examined.

II. VIRTUAL CRYSTAL (VC) APPROXIMATION

A. Overview

Abelès first introduced the idea of using a virtual crystal (VC) to replace a disordered one, computing the thermal conductivity of Si/Ge alloys by treating both disorder and anharmonicity as perturbations.¹¹ Many experimental trends in thermal conductivity of a range of materials can be explained using the VC approximation.(cite) For example, the reduced thermal conductivity of Ge versus Si and Si/Ge alloys is partly explained by both the increased mass and decreased bulk modulus (stiffness) of the lattice.(cite) Both have the effect of reducing phonon group velocities. (cite) However, a complete description of the thermal transport in alloys requires modeling in-

trinsic and disordered scattering to calculate phonon lifetimes (see Section II E 2).

Phonon lifetimes can be predicted by treating both the intrinsic and disorder scattering using perturbation theory (Section). While the theory which treats phonon defect scattering (Eq.) is valid for perturbative disorder, its use leads to good agreement with several experimental and computational results with large disorder. Cahill shows that conductivity reduction in dilute Ge-doped Si epitaxial layers is captured by mass perturbative disorder.⁷ While the mass disorder was large ($m_{Ge}/m_{Si} = 2.6$), the overall disorder strength is dictated by the concentration. As little as $6.2 \times 10^{19} cm^{-3}$ Ge ($g = 3.1 \times 10^{-3}$, Section) is enough to reduce the thermal conductivity of Si by almost a factor of 2.¹² In the case of the $Ni_{0.55}Pd_{0.45}$ alloy, the atomic species are chemically similar but both the mass disorder ($m_{Pd}/m_{Ni} \approx 2$) and concentration are large ($g = 0.078$) and good agreement is also seen using a VC approach.¹³

Computational results using the VC approximation for moderate to high thermal conductivity alloys show good to excellent agreement with experimental results^{4?}⁵. Garg used ab initio calculations with VC-ALD (Section) to predict the thermal conductivity of Si/Ge alloys for all concentrations, obtaining excellent agreement with experiment.⁵ Lindsay and Broido found good agreement with VC-ALD and experiment for isotopically defected GaN.⁴ Both Si/Ge and isotopically defected GaN have relatively large thermal conductivities, even for large concentrations. A detailed study of low thermal conductivity materials PbTe⁶ and PbTe/PbSe⁷ made predictions for the perfect systems in fair agreement with experiment, but where results lack for the alloys. Thus, there is a need to examine the perturbative approach VC-ALD for heavily disordered systems. The computational studies discussed above were limited to the use of VC-ALD because of the computational cost of ab initio calculations. Using empirical potentials, we study the effects of explicit disorder in Section .

Using the VC approximation, we perform calculations at different concentrations (c) of mass varying ($m_{1-c}^a m_c^b$) binary alloys of LJ argon and SW silicon (Section). Using the VC approximation, the phonon mode properties of the VC (frequencies (Section) and group velocities (Section)) and predict lifetimes (Section) and thermal conductivity (Section). Methods referred to as VC-NMD (Section) and VC-ALD (Section) use the VC approximation. Explicit disorder is examined using lattice dynamics (LD) calculations (Section) and molecular dynamics (MD) simulations (Section) of explicitly disordered supercells (Section).

B. Kinetic Theory

For a perfect system, all vibrational modes are phonons, which by definition are delocalized, propagating plane waves.(cite) Using the single-mode relaxation

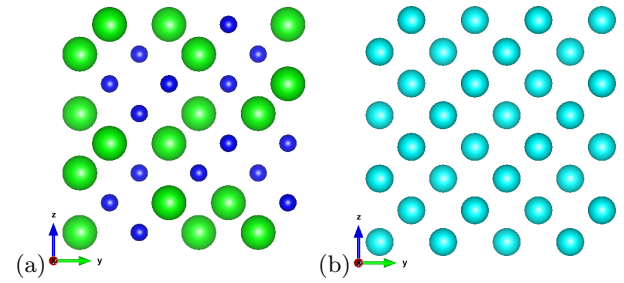


FIG. 1: (a) view of a [010][001] plane of an explicitly disordered supercell of Si and “heavy” Si ([100] direction into the paper).¹⁴ (b) view of a [010][001] plane of the VC supercell with an average mass of the explicitly disordered Si and “heavy” Si supercell (b). Sphere size represents increasing mass only, no bond disorder is considered. In this work, calculations for LJ Ar and SW Si which use the VC approximation are based off of the conventional cubic unit cells (Section II C, II D 1, II E 1 and II E 2), which build the lattice of the perfect (a) and disordered supercells (b). Disorder is taken into account explicitly using the disordered supercells in Sections II C, II D 2, II E 1 and ??.

time approximation¹⁵ as an approximate solution of the Boltzmann transport equation¹⁶ gives an expression for thermal conductivity,

$$k_{ph,\mathbf{n}} = \sum_{\boldsymbol{\kappa}} \sum_{\nu} c_{ph}(\boldsymbol{\kappa}) \mathbf{v}_{g,\mathbf{n}}^2(\boldsymbol{\kappa}) \tau(\boldsymbol{\kappa}). \quad (1)$$

Here, the phonon mode has frequency $\omega(\boldsymbol{\kappa})$ (Section), c_{ph} is the phonon volumetric specific heat, $\mathbf{v}_{g,\mathbf{n}}$ is the component of the group velocity vector in direction \mathbf{n} (Section), and $\tau(\boldsymbol{\kappa})$ is the phonon lifetime (Section). Since the MD simulations we perform (Section) are classical and obey Maxwell-Boltzmann statistics,¹⁷ the specific heat is k_B/V per mode in the harmonic limit, where V is the system volume. This approximation has been shown to be valid for LJ Ar(cite SED or ASME?) and SW Si(cite SED or ASME?) and is used for all calculations in this work so that direct comparisons can be made for all methods. (cite SED or AMSE?) For the perfect and disordered lattices studied in this work, the thermal conductivity is isotropic so we refer to k_{ph} only.

For heavily disordered systems, the Allen-Feldman theory computes the contribution to vibrational conductivity by diffuson modes (Section).³⁸

Studies have attempted to quantify the relative contribution of both phonons and diffusons to the total vibrational conductivity, $k_{vib} = k_{ph} + k_{AF}$.²⁵

energy transport in jammed sphere packings?
heat transport in model jammed solids?

C. VC and Gamma DOS

In this section, we examine the effect of explicit disorder by computing the density of states (DOS, $D(\omega(\kappa_\nu))$) for vibrational modes of the VC and of explicitly disordered supercells. Perfect and explicitly disordered supercells are generated with atomic positions based on LJ argon's FCC and silicon's diamond-FCC ($b \leq 8$) crystal structure using randomized masses. The composition is labeled by $m_{1-c}^a m_c^b$, where $m^a = 1$ and $m^b = 3$ in LJ units for argon and $m^a = m_{Si}$ and $m^b = 2.6m_{Si}$ for SW silicon and "heavy silicon" (mass of germanium). For $c = 0.5$, the LJ VC has average mass of 2.

Supercells are built cubically with size N_0 , where N_0 refers to the number of repetitions of the unit cell in all 3 spatial directions.(cite) Supercells up to size $N_0 \leq 12$ for LJ argon (6096 atoms) are used for calculations. For SW silicon, $N_0 \leq 10$ (SW silicon, 8000 atoms) are used for the MD-based methods and $N_0 \leq 24$ for VC-ALD. The lattices are generated using the cubic conventional unit cells of the FCC ($n = 4$) and diamond-FCC ($n = 4$) crystals (where n the number of atoms in the unit cell).

The supercells are built using the zero-pressure finite-temperature lattice constants for LJ argon, which are $a = 1.556$ (T=10K) and $a = 1.580$ (T=40 K) in LJ units. For LJ argon, the variation of lattice constant with composition is small and ignored. The effective zero-pressure finite-temperature lattice constant of the amorphous phase at T=10K is slightly larger ($a = 1.585 = (1/n_v)^{1/3}$ where n_v is the number density, Section) and does not exist above approximately $T = 20K$.⁷ All LJ calculations use these lattice constants. For SW silicon, the lattice constant $a = 5.43\text{\AA}$ is used for all calculations, which brings the GK thermal conductivity predictions¹⁹ into better agreement with VC-ALD²⁰, particularly for $c = 0.0$ (Section).

Each vibrational mode contributing to the thermal conductivity has a frequency $\omega(\kappa_\nu)$. The allowed frequencies are the square root of the eigenvalues of the system's Dynamical matrix, $D(\kappa)$,¹⁸ which relates the mode eigenvector ($e(\kappa_\nu^b)$) and eigenvalue by

$$D(\kappa)e(\kappa_\nu^b) = \omega^2(\kappa_\nu) e(\kappa_\nu^b). \quad (2)$$

In a perfect system all vibrational (normal) modes are plane-waves, and as such can be identified by a wavevector κ , eigenvector $e(\kappa_\nu^b)$, and a possibly degenerate frequency $\omega(\kappa_\nu)$. Here, b labels the atom in the unit cell, α labels the cartesian coordinates, and ν labels the mode polarization (possibly degenerate in frequency). In a disordered system, such as a crystal lattice with randomly arranged and differing mass species, all normal modes exist at the wavevector [000], where $b \leq N_a$ and $\nu \leq 3N_a$, where N_a is the total number of atoms in the system. In general, normal modes in a disordered system will not be pure plane-waves and will be non-degenerate in frequency. We compare the ordered and disordered normal mode frequencies in Section ?? and mode eigenvectors in Section .

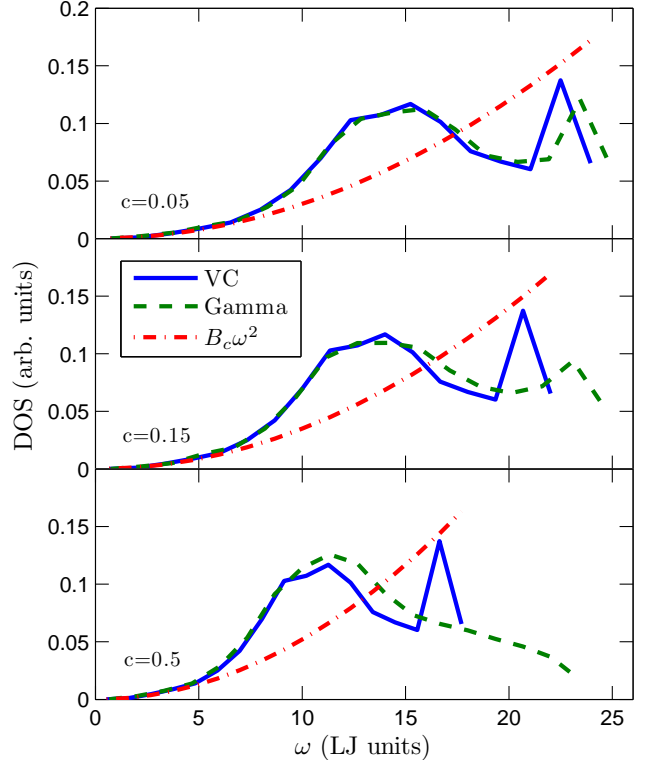


FIG. 2: Density of states (DOS) for modes calculated using the LJ FCC VC versus an explicitly mass disordered LJ FCC supercell (labeled Gamma) with varying mass concentration c (Section). VC and Gamma show similar low frequency behavior for all c . For increasing c , the frequencies of both VC and Gamma decrease, while the high frequency DOS for Gamma spreads and reaches up to a higher maximum frequency because of the explicit disorder. The size of these supercells is $N_0 = 12$ (see Section).

With the appropriate dynamical matrix ($\kappa = [000]$ for the explicitly disordered supercells), the frequencies are computed using the program GULP.²¹ For the VC, the frequencies are identified (up to polarization) by the list of wavevectors allowed by the size of the supercell.(cite) The DOS for the VC and the explicitly disordered supercells (referred to as Gamma) are shown in Fig. The frequencies agree between VC and Gamma at low frequencies, where the Debye approximation predicts $DOS(\omega) \propto \omega^2$.(cite) The increasing lattice mass with increasing c for the VC has the effect of reducing the frequencies. The increasing lattice mass for the Gamma modes also has the effect of reducing the frequencies. However, the effect of explicit disorder can be seen at high frequencies by a broadening and a shift of the DOS to higher frequencies because of the explicit light atoms used in the supercell. Similar agreement at low frequencies was found in ab initio predictions for Si_cGe_{1-c} ,⁵ while Bouchard showed similar behavior for a- Si_cGe_{1-c} .²²

D. Phonon Group Velocities

1. From VC Dispersion

The group velocity vector in a VC is the gradient of the dispersion curves (i.e., $\partial\omega/\partial\kappa$), which can be calculated from the frequencies and wavevectors using finite differences. In this work, the group velocities for the VC are calculated using finite difference and quasi-harmonic lattice dynamics.⁷ While the group velocities are necessary to predict the thermal conductivity, of particular interest is the phonon mean free path (MFP), $\Lambda(\kappa) = |\mathbf{v}_g|\tau(\kappa)$, which is crucial for understanding nano and micro-nanostructuring effects.(cite) Thus, predicting group velocities in disordered systems is just as crucial as predicting mode lifetimes.(cite)

Except for the three acoustic branches (2 transverse, 1 longitudinal), there is not an accepted method to calculate the effective group velocity of a vibrational mode in a disordered system. though there are attempts.^{23–26} Dispersion for a model 1D system demonstrated the effect of disorder on the group velocity in terms of a zone-folding effect.²³ In studies of disordered silicon systems, the group velocity of vibrational modes was estimated using an interpolation scheme for small but finite wavevectors around [000].^{24–26} We do not, in general, observe the required dispersion behavior to perform this interpolation for the LJ and SW systems studied in this work. Feldman et al used the structure factor to predict an effective dispersion for a model of a-Si, but did not predict group velocities.(cite) Volz and Chen used the dynamical structure factor to predict the dispersion of SW Si using MD simulation, but in a perfect system.⁷ We examine the structure factor for the explicitly disordered modes in the next section.

2. From Structure Factor of Gamma Modes

Measuring the explicitly disordered (Gamma) mode's structure factor is a method to test for the plane-wave character of modes at a particular wavevector and polarization.(cite) The structure factor is defined as²⁷

$$S^{L,T}(\kappa) = \sum_{\nu} E^{L,T}(\nu) \delta(\omega - \omega(\nu)), \quad (3)$$

where E^T refers to transverse polarization and is defined as

$$E^L(\nu) = \left| \sum_{l,b} \hat{\kappa} \cdot e(\nu b) \exp[i\kappa \cdot \mathbf{r}_0(l_b)] \right|^2 \quad (4)$$

and E^L refers to longitudinal polarization and is defined as

$$E^T(\nu) = \left| \sum_{l,b} \hat{\kappa} \times e(\nu b) \exp[i\kappa \cdot \mathbf{r}_0(l_b)] \right|^2. \quad (5)$$

Here, $\mathbf{r}_0(l_b)$ refers to the lattice positions in the mass disordered supercells which are still spatially ordered. Explicit disorder is accounted for in the mode frequencies $\omega(\nu)$ and eigenvectors $e(\nu b)$ which are calculated with $\kappa = [000]$.

Physically, $S^{L,T}(\kappa)$ calculates the frequency spectrum required to create a wavepacket with well-defined wavevector and polarization. In a perfect system the structure factor peaks are delta functions centered at the mode frequencies. With increasing disorder (c), the structure factor spreads in width, particularly at high frequencies (Fig.). An effective dispersion can be extracted by locating the peaks in the structure factors, where the effects of polarization, virtual mass, and anisotropic dispersion can be observed (Fig.). As the lattice VC mass becomes larger, the peaks in the structure factor shift to lower frequencies. The peaks in the structure factor are shifted to slightly higher frequencies than the VC predicted frequencies by up to only %5. Because of this, we use the group velocities predicted by the VC dispersion in both our VC-NMD and VC-ALD calculations for consistency and simplicity.

To calculate the $S^{L,T}(\kappa)$ for a finite size system, the delta function in Eq. (??) is broadened using a Lorentzian function with a full-width at half maximum $\Gamma_{FMHW} = \delta_{\omega,avg}$, where $\delta_{\omega,avg}$ is the average frequency spacing. Allen et al²⁷ demonstrated using a model of a-Si that the structure factor for large wavevector broadens such that the linewidth $\Gamma_{SF} > \omega$ such that the peaks no longer propagate. For the systems sizes studied, Γ_{SF} scale with the broadening factor Γ_{FMHW} for all peaks except those at high frequencies. The lifetimes ($\tau_{SF} = 1/2\Gamma_{SF}$) of the structure factor peaks at high frequency are in better agreement with the lifetimes at high frequency predicted by VC-NMD rather than VC-ALD, where generally $\tau > 2\pi/\omega$ (Ioffe-Refel limit, Fig.).²⁸ This gives more justification for the use of the VC predicted group velocities even for large wavevector and large c .

Well-defined peaks at all wavevectors are most likely due to the spatial lattice structure of the disordered systems studied in this work. Typically, the structure factor for amorphous materials has well-defined peaks only for small wavevector.²⁷ The group velocity of moderate to high frequency modes in a 1D alloy are drastically reduced by considering the effects of zone folding.²³ Based on the results using the structure factors in Fig., the reduction due to zone folding would seem to underpredict the group velocity of moderate to high frequency modes. This ambiguity can be resolved by considering the thermal diffusivity of a given mode, which incorporates the variation of both group velocity and lifetime (see Section).

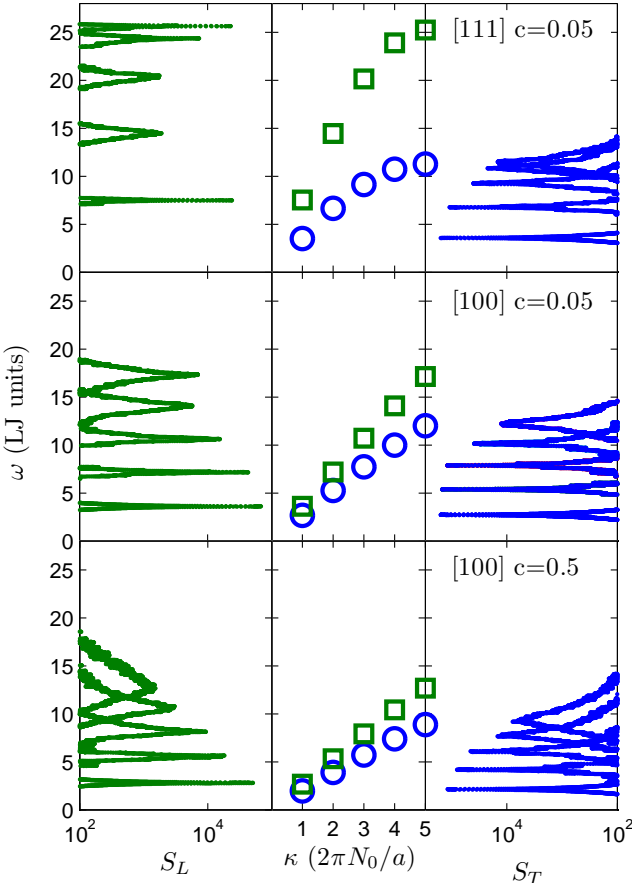


FIG. 3: Left and Right Panels: The structure factor for longitudinal (S_L) and transverse (S_T) polarizations along high symmetry directions ([100], [110] where $\kappa = \pi/a[100]$ and a is the lattice constant) of the mass disordered LJ FCC supercells ($c = 0.05, 0.5$). For increasing mass disorder c , there is a decrease in the center of the peaks and an increase in the peak linewidths. Center Panel: The VC predicted dispersion at the same wavectors used to calculate $S_{L,T}$.

E. Phonon Lifetimes

1. From VC-NMD and Gamma

As an alternative to the VC-ALD models for predicting phonon lifetimes (Section), we use the normal mode decomposition (NMD) method.(cite) NMD maps the atomic trajectories (positions and velocities) of all atoms in an MD simulation onto vibrational normal modes.(cite) The MD simulation is performed using the perfect (VC) and disordered (Gamma) supercells (Section, Fig.). The lifetimes are predicted using the frequencies and eigenvectors from both the VC ($\omega(\kappa)$, $e(\kappa^b_\alpha)$) and the Gamma supercell ($\omega(\kappa)$, $e(\kappa^b_\alpha)$ with $\kappa = [000]$). The vibrational mode frequencies and eigenvectors are necessary for the mapping of the atomic tra-

jectories from the MD simulation onto the vibrational normal mode coordinates, $q(\kappa; t)$ and $\dot{q}(\kappa; t)$, which are required to calculate the total vibrational normal mode energy $E(\kappa)(t)$.(cite)

The normal mode lifetime is predicted using

$$\tau(\kappa) = \int_0^\infty \frac{\langle E(\kappa; t) E(\kappa; 0) \rangle}{\langle E(\kappa; 0) E(\kappa; 0) \rangle} dt. \quad (6)$$

For a normal mode which is an exact normal mode of the system, the autocorrelation of the total and kinetic normal mode energy are cosinusoidally damped exponentials with a decay time $\tau(\kappa)$ and a single oscillation frequency $2\omega(\kappa)$.(cite joe) In Fig. , the

The effects of disorder enter through the atomic trajectories of the MD simulation.

When using the VC normal modes to map the trajectories for the explicitly disordered system, the mode total and kinetic energy do not follow these simple functional forms. This can be understood by using spectral NMD in the frequency domain, where multiple peaks in an isolated mode's energy spectrum (Φ) can be observed (see Fig.).(cite) In the case of multiple peaks, the choice of which to fit can be ambiguous. However, a lifetime can be predicted unambiguously using Eq. even with these multiple-peak artifacts. These artifacts are not surprising given two considerations: 1) the MD simulations contain explicit disorder which influences the atomic trajectories 2) the normal modes are mapped without using the exact eigenvectors and frequencies of the explicitly disordered system.

The lifetimes predicted using the VC approximation and the Gamma supercells are shown in Fig. First, the frequencies of the modes for VC-NMD and Gamma differ slightly, particularly at high frequency, which is demonstrated by the difference in the DOS (Fig.). For a small intervals of frequency, there are a wider range of predicted lifetimes for Gamma. This is because there is no symmetry averaging of the mode properties, which is performed for the modes of the VC.

Discrepancies have been observed previously when the exact normal modes of the system are not used.(cite jason) However, the lifetimes predicted using VC-NMD are in fairly good agreement with those calculated using Gamma (Fig.). Several studies have found good agreement for predictions of lifetimes and thermal conductivity using non-exact eigenvector mappings^{9,29} in a wide-range of materials and phonon scattering conditions.^{8,9,29-31} However, it is crucial that results using non-exact mappings are compared to as many alternative methods as possible. In this work, VC-NMD is compared to the other methods Gamma (Section), GK (Section), and VC-ALD (Section). It is important to remember that the VC normal modes are exact in the limit $c \rightarrow 0$. Use of the VC modes at large c pushes the limits of the approximation, but also is useful for predicting an effective group velocity (Section).

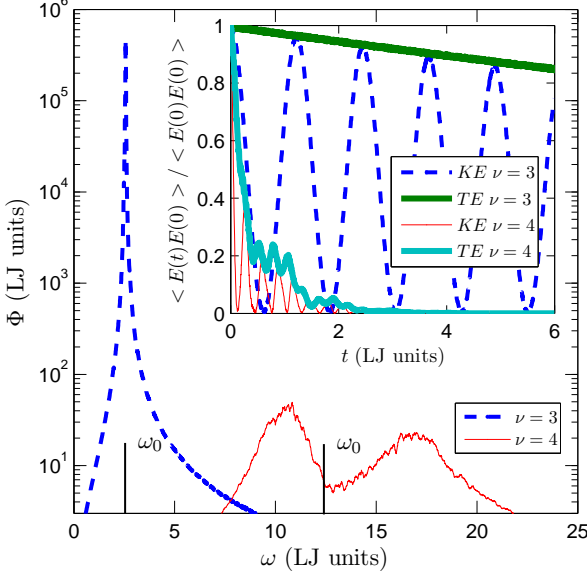


FIG. 4: The spectral energy density Φ of two modes (polarizations $\nu = 3, 4$ at wavector $[0.2 \ 0 \ 0]$) calculated using VC-NMD for a mass disordered LJ FCC supercell ($N_0 = 8$ and $c = 0.5$, Section). The VC dispersion-predicted peaks are labeled by ω_0 . Inset: the same mode's energy (kinetic (KE) and total (TE)) autocorrelation functions. Note the additional harmonic effects in the KE and TE autocorelation functions for $\nu = 4$ which are due to the double peaks in Φ . A mode lifetime can be extracted unambiguously using the integral of the TE autocorrelation function (Section).

2. From VC-ALD

Assuming the intrinsic and disorder scattering mechanisms to operate independently, the effective phonon lifetime can be found using Matthiessen's rule(cite),

$$\frac{1}{\tau(\boldsymbol{\kappa})} = \frac{1}{\tau_{p-p}(\boldsymbol{\kappa})} + \frac{1}{\tau_d(\boldsymbol{\kappa})}, \quad (7)$$

where $\tau_{p-p}(\boldsymbol{\kappa})$ accounts for phonon-phonon scattering, $\tau_d(\boldsymbol{\kappa})$ accounts for boundary scattering, $\tau_d(\boldsymbol{\kappa})$ accounts for defect scattering.

Phonon-phonon scattering ($\tau_{p-p}(\boldsymbol{\kappa})$) is typically treated using anharmonic perturbation theory (ALD) including only 3-phonon processes.^{5,7,32} It has been estimated that the effects of higher order phonon processes are small³³, particularly at low temperatures.³² At low frequencies, $\tau_{p-p}(\boldsymbol{\kappa})$ follows a scaling due to both normal ($B_1\omega^2$) and umklapp ($B_2\omega^2$) 3-phonon scattering processes, where the density of states is Debye-like(cite) and the constants B_1 and B_2 are typically fit to experimental data. The scaling $\tau \propto \omega^{-2}$ can be observed in both the NMD (Fig.) and ALD (Fig.) predicted results.

Using harmonic perturbation theory, Tamura gives a

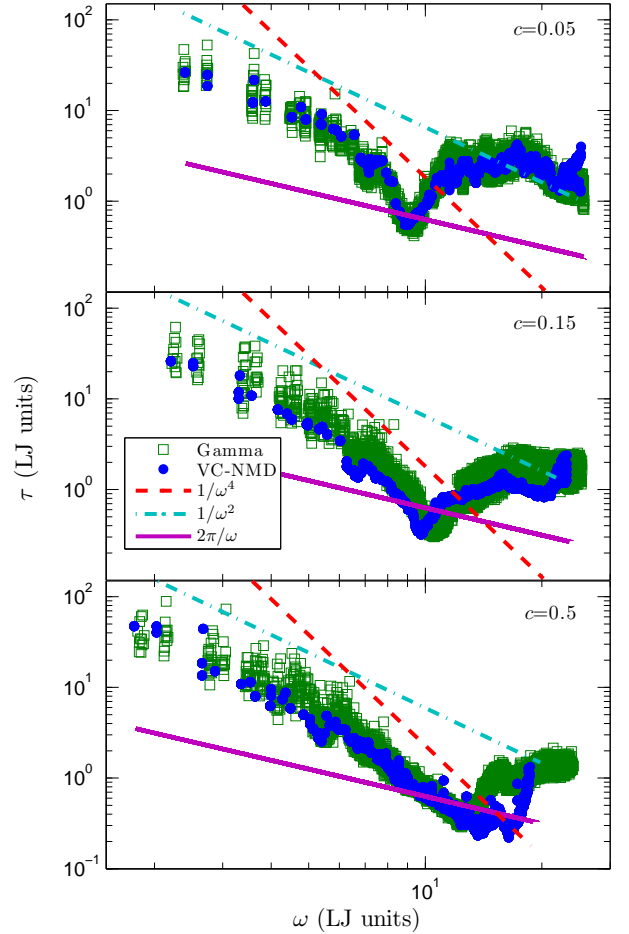


FIG. 5: Lifetimes predicted using VC-NMD and Gamma NMD from MD simulations of mass disordered FCC supercells (Section). Both ω^{-2} and ω^{-4} scalings can be observed at low frequencies, which are predicted by the perturbative models used for VC-ALD (Section). For both VC-NMD and Gamma NMD, most mode lifetimes are greater than the Ioffe-Regel limit $\tau = 2\pi/\omega$.²⁸ While there is more “noise” in the Gamma mode data because of the symmetry averaging of the VC-NMD modes (Section), the lifetime magnitudes and trends agree well, an important consideration when comparing VC-NMD and VC-ALD in Fig. .

general expression for mass point defect scattering³⁴

$$\frac{1}{\tau_d(\boldsymbol{\kappa})} = \frac{\pi}{2N} \omega^2(\boldsymbol{\kappa}) \sum_{\boldsymbol{\kappa}' \boldsymbol{\nu}'} \delta(\omega(\boldsymbol{\kappa}) - \omega(\boldsymbol{\kappa}')) \sum_b g(b) |e^*(\boldsymbol{\kappa}' \boldsymbol{\nu}') \cdot e(\boldsymbol{\kappa} \boldsymbol{\nu})|^2, \quad (8)$$

where $g(b) = \sum_\mu c^\mu(b)(1 - m^\mu(b)/\bar{m}(b))^2$, N is the number of unit cells, and c^μ is the concentration, $m^\mu(b)$ is the mass of the μ -th species and \bar{m}^μ is the average mass. For the binary alloys considered, there is one atom type in the unit cell ($b = 1$ only) with $\mu = a, b$, such that

the alloying atom labeled by m_{1-c}^b can be considered to be an “isotope” of atom labeled m_c^a . This convention is appropriate because of the perturbative approach used to derive Eq. , while we consider large disorder of up to $c = 0.5$.³⁴

By considering the symmetry properties of the FCC lattices considered in this work (Section), it can be shown that $1/\tau_d(\kappa_\nu) = \frac{\pi}{2} g \omega^2(\kappa_\nu) D(\omega(\kappa_\nu))$, where $D(\omega(\kappa_\nu))$ is the density of states (Section) and g is the disorder coupling strength.³⁴ Under the Debye-approximation ($D(\omega(\kappa_\nu)) \propto \omega^2$), the phonon scattering due to mass point-defects is given by $A\omega^{-4}$, where A is a constant related to the unit cell volume, branch-averaged group velocity, and disorder coupling strength (g in Eq. above). The frequency dependence (ω^4) is the same as Rayleigh scattering, which is valid at low frequency and observed in both the NMD (Fig.) and ALD (Fig.) predicted results.

The disorder scattering scaling is expected to fall off faster than ω^{-4} when $D(\omega(\kappa_\nu))$ grows faster than the Debye scaling of ω^2 (Fig. , Section). The lifetimes do fall off faster ω^{-4} for the mass disordered LJ FCC supercells for a narrow range of frequencies near $\omega = 10$ in Fig. for $c = 0.05, 0.15$, but seem to follow more closely ω^{-4} for $c = 0.5$.

Bond disorder can be accounted for using a similar expression with an average atomic radius or suitable scattering cross-section.^{35,36} The effect of bond and mass disorder has been investigated computationally by Skye and Schelling for Si/Ge³⁷, where it was shown that mass disorder is the dominant scattering mechanism. In this work we consider only mass disorder.

For the VC-ALD method, the intrinsic $\tau(\kappa_\nu)_{p-p}$ is calculated using the method described in.³² To calculate the disordered lifetimes $\tau(\kappa_\nu)_d$ (Eq.), it is necessary to broaden the δ function using a Lorentzian function. For all calculations, the Lorentzian was broadened using a value of 100 times the mean level spacing. For the system sizes here, the results do not differ significantly if this broadening value is varied by changing it manually or making the system size (N_0) bigger.

F. Vibrational Mode Diffusivity

The diffusivity section was a bit hard to follow.

In the classical limit, where the specific heat $c_p(\kappa_\nu) = k_B$, a vibrational mode’s contribution to thermal conductivity is determined by the mode thermal diffusivity. For phonons, the thermal diffusivity is

$$D_{ph}(\omega(\kappa_\nu)) = v_{g,n}^2(\kappa_\nu) \tau(\kappa_\nu). \quad (9)$$

We now compare the phonon mode diffusivities, $D_{ph}(\omega(\kappa_\nu))$ predicted by both VC-NMD and VC-ALD to the proposed lower limit $D_{AF,HS} = (1/3)v_s a$ (see Section). Here, a is 1/2 the lattice constant of the cubic conventional unit cells used for both FCC LJ argon

and diamond-FCC SW silicon, although the choice of this length scale is not unique. For the a value in Eqs. (12)-(14), why not use the bond length?

For LJ argon, VC-NMD predicts lifetimes which are generally larger than the period ($2\pi/\omega(\kappa_\nu)$) of the vibrational oscillation (Ioffe-Regel limit)(cite), and actually increase high frequency for small intervals (Fig. and). VC-NMD predicts larger phonon lifetimes at high frequency compared to VC-ALD (Fig.), which predicts essentially monotonically decreasing lifetimes with increasing frequency. Because VC-NMD and VC-ALD use the same values for $v_g(\kappa_\nu)$, the phonon mode diffusivities D_{ph} are also underpredicted by VC-ALD compared to VC-NMD. This leads to an underprediction for VC-ALD of both the thermal conductivity spectrum (Fig.) at high frequency and the total thermal conductivity (Fig.) compared to VC-NMD.

For both VC-NMD and VC-ALD, a significant number of modes have $D_{ph}(l; t) D_{AF,HS}$. This leads to an underprediction of the total thermal conductivity compared to GK (Fig.). The diffusivity of these modes can be adjusted such that any mode with $D_{ph}(l; t) D_{AF,HS}$ is given $D_{ph} = D_{AF,HS}$. The result of this adjustment, referred to as VC-NMD* and VC-ALD*, is examined in the next section.

The energy diffusivity, d , quantifies how far a wave packet narrowly peaked at a frequency can propagate.³⁸ ?

A heuristic argument for the relation between d and T is as follows. For a system in a temperature gradient, it is well known that the heat diffusivity obeys the relation $d = V / C$. Thus, $= dC / V$. This relation can be generalized mode by mode.

In amorphous systems, the diffusivities themselves can be combined using a Matthiesen-like expression (multiple resistors in series).?

The mode lifetime typically diverges as $\omega - \omega_c > 0$ because the vibrational modes are long-wavelength plane waves (phonons) that weakly scattered by the disorder.?

In fact, the low-temperature behavior of glasses is described?

At very low frequency, the mode diffusivities for phonons or diffusons can be factored as the product of the sound speed, $D_{ph} = v_s^2(\kappa_\nu) \tau(\kappa_\nu)$ and $D_{AF} = (1/3)(v_s)^2 \tau_{AF}$.

The key difference is that for the lattices studied in this work, for $c = 0$ there is dispersion such that $v_g(\kappa_\nu)$ instead of $v_g(\kappa_\nu) = v_s$ as in the Cahill-Pohl model. For perturbative disorder ($c = 0.05$ Fig.), the narrow peaks of the disordered lattice’s structure factor (Section) suggest that the

This perplexing property of glasses has been explained heuristically by assuming that phonons are scattered so strongly by structural disorder that transport becomes diffusive, with a frequency regime of small, constant thermal diffusivity? ?

By contrast, T is generally infinite if anharmonic corrections are ignored. This is because d in the inte-

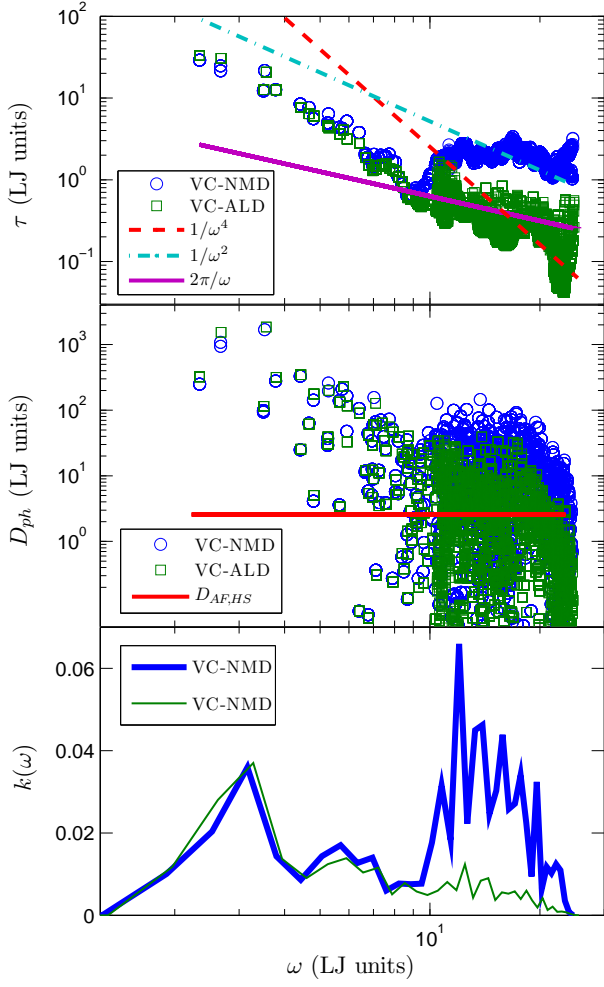


FIG. 6: gamma point results

grand of Eq. 4 diverges too strongly at low frequencies due to phonons that are progressively less scattered with increasing wavelength.⁷ In order to cure this divergence, additional scattering mechanisms, beyond harmonic theory, are typically invoked resulting in an additional contribution to the diffusivity, d_c

In heavily disordered systems, such as large c alloys or glasses, modes can transport heat by harmonic coupling due to the disorder in the Allen-Feldman (AF) theory of diffusons.³⁸ In the classical limit, the AF thermal conductivity is written as

$$k_{AF} = \sum_{\omega} \frac{k_B}{V} D_{AF}(\omega(\kappa)), \quad (10)$$

where V is the system volume and $D_{AF}(\omega_{AF})$ is the thermal diffusivity of the mode labeled by frequency $\omega(\kappa)$ with ν ranging over all modes in the disordered supercell and $\kappa = [000]$.(cite)

In a weakly scattering system, $D_{AF} = v_s \tau(\omega)/3$ ⁷

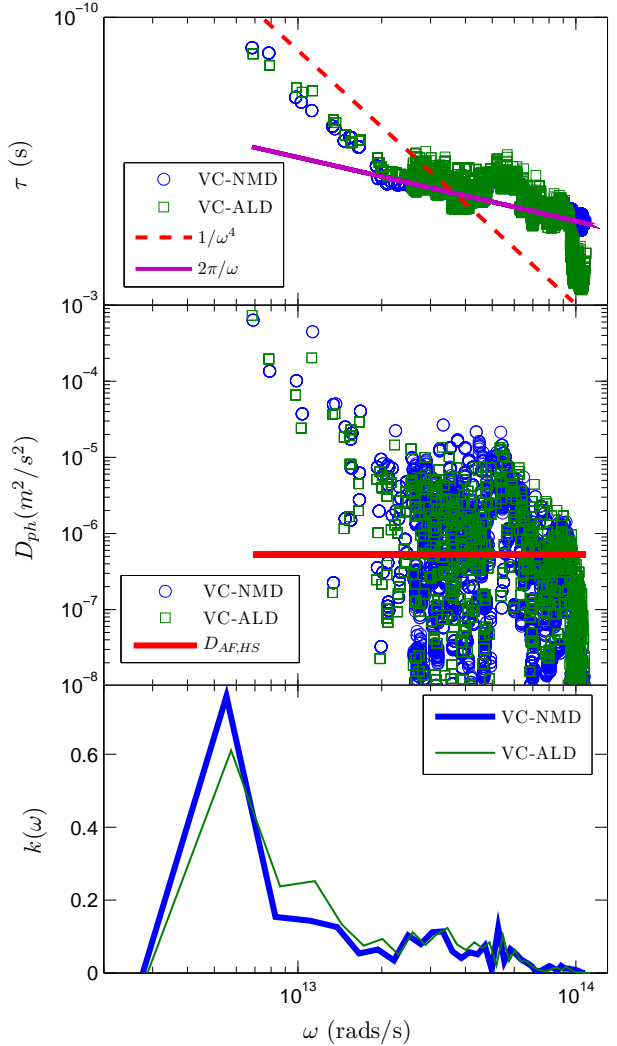


FIG. 7: gamma point results

In fact, for a-Si, the mode diffusivities do vary as a function of frequency, which is used to explain the propagating mode effects seen in a-Si thin films.(cite)

In the high-scatter (HS) limit,(cite) the AF diffusivity of each mode is

$$D_{AF,HS} = \frac{1}{3} v_s a. \quad (11)$$

A similar HS limit for mode diffusivity is given by the Cahill-Pohl (CP) model,(cite)

$$D_{CP,HS} = 0.403 v_s a. \quad (12)$$

The CP thermal conductivity prediction in the HS limit is

$$k_{CP,HS} = \left(\frac{\pi}{6}\right)^{1/3} \left(\frac{3}{2}\right) \frac{k_B}{V_b} b v_s a, \quad (13)$$

where V_b is the volume of the unit cell, v_s is the branch-averaged sound speed, and a is the lattice constant (or

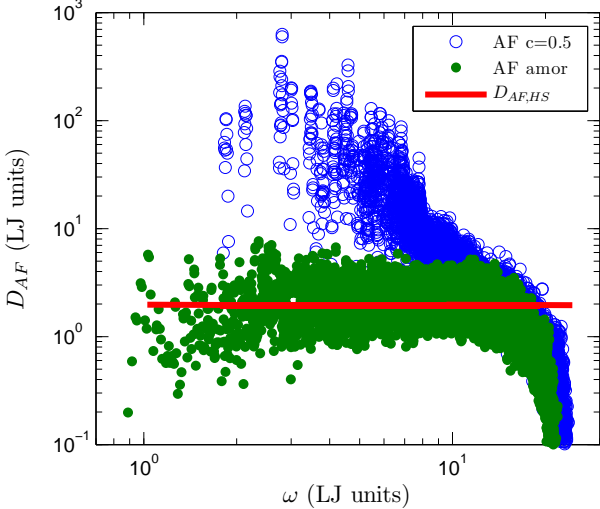


FIG. 8: gamma point results

appropriate length scale).³⁹ Comparing with Eq., the AF,HS limit predicts a mode diffusivity and thermal conductivity which is approximately %20 smaller than CP,HS.³⁹ Ignoring this small difference, the interpretation for both $D_{AF,HS}$ and $D_{CP,HS}$ is of a vibrational mode with a group velocity equal to the sound speed and mean-free path equal to the lattice spacing. While the CP,HS model assumes $\tau(\kappa) = 1/\omega(\kappa)$ and $v_g = v_s$ for all modes, the AF theory is capable of predicting the mode diffusivities without any assumptions other than a harmonic approximation.(cite)

With sufficient disorder, the harmonic AF theory is capable of accurately predicting a finite thermal conductivity.^{40,41} However, the AF theory does not treat the intrinsic anharmonic scattering of low frequency phonon modes, where in the infinite-size the AF conductivity of a disordered lattice is divergent.(cite) While the low frequency modes are not treated properly in the harmonic AF theory, the mode diffusivities D_{AF} of high frequency modes in the heavily disordered ($c = 0.5$) LJ FCC supercell approach that of similar frequency modes in the amorphous phase (Fig.). footnote(The amorphous LJ phase was created by liquifying the crystal and instantly quenching by removing all kinetic energy. The resulting structure was then energy minimized and annealed in an NPT ensemble at zero pressure and $T = 10$ K.(cite lammps) In the amorphous phase, modes with significant contribution to thermal transport can be modeled using a mode-independent diffusivity of $D_{AF,HS}$ (Eq.). In fact, the difference between $k_{AF} = 0.099W/m = K$ and $k_{HS,CP} = 0.124$ is approximately %20. This places a plausible lower-bound on the value of the phonon mode diffusivities, $D_{ph} \geq D_{AF,HS}$, predicted by VC-NMD and VC-ALD in the following section.

III. THERMAL CONDUCTIVITY PREDICTIONS

An addition of as little as 10% Ge is sufficient to reduce the thermal conductivity to the minimum value achievable through alloying. Theoretically, mass disorder is found to increase the anharmonic scattering of phonons through a modification of their vibration eigenmodes. Notably, the thermal conductivity is found to drop sharply after only a small amount of alloying. This is due to the strong harmonic scattering of phonons even in the dilute alloy limit.

Duda shows that taking a perfect alloy and disordering via an order parameter allows control of thermal conductivity.⁴²

In fact, the beginning breakdown of the intrinsic scattering model ($\tau_{p-p}(\kappa)$) can be observed for the perfect ($c = 0.0$) crystal at $T = 40$ K (see Fig.), where ALD begins to overpredict compared to GK. This can be explained by the emerging importance of higher order ($n > 3$) n-phonon process at high temperatures.³²

For LJ argon, bulk thermal conductivity predictions are made for VC-NMD, VC-ALD and GK (Fig.). For SW silicon, bulk thermal conductivity predictions can only be made for VC-ALD and GK (see Appendix). For LJ argon, both VC-NMD and VC-ALD underpredict the thermal conductivity compared to GK. By adjusting the mode diffusivity $VC - NMD*$ and $VC - ALD*$.

IV. DISCUSSION

While the models presented in, there is no theoretical justification for the lower limit to the mode mean-free path.⁷ For the lattices studied in this work, the more appropriate quantity to consider is the mode diffusivity since both the effective mode lifetime and group velocity are varying with frequency (Fig.). Since the Allen-Feldman theory does not rely on the assumption of propagating phonons we expect the results for d to be valid even in the high-frequency regime, where the diffusivity cannot be factorized into a product of $l(\omega)$ times a frequency-independent speed of sound.

For $c = 0$ the group velocities are given from the dispersion (Section).

In these ordered and disordered lattices, it is difficult to separate the contributions to the total vibrational conductivity from $D_{ph}(\kappa)$ and D_{AF} unless the lower limit $D_{CP,HS}$ or $D_{AF,HS}$ are used.

While the expression for harmonic defect scattering (Eq.) is valid for perturbative disorder, its use leads to good agreement with several experimental and computational results with large disorder. Cahill shows that conductivity reduction in dilute Ge-doped Si epitaxial layers is captured by mass perturbative disorder.⁴³ In this case, the mass disorder is large ($m_{Ge}/m_{Si} = 2.6$) but the overall disorder strength is dictated by the concentration. For example, as little as $6.2 \times 10^{19} cm^{-3}$ Ge ($g = 3.1 \times 10^{-3}$)

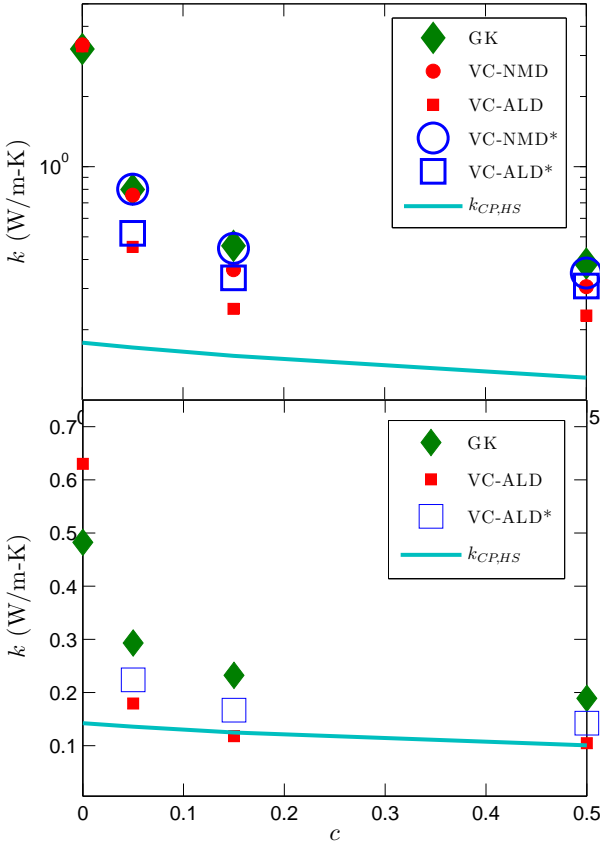


FIG. 9: The vibrational conductivity of LJ alloys predicted using MD simulations and the Green-Kubo method. The predicted thermal conductivities are for a LJ alloy of the form $m_{1-c}^a m_c^b$, where $m^a = 1$, $m^b = 3$, and $m_r = m^a/m^b = 3$ (in LJ units). As the alloy concentration is increased perturbatively, the vibrational conductivity drops quickly and saturates to a minimum at $c = 0.5$. For $c = 0.5$ the system is heavily disordered and the vibrational conductivity approaches that of an amorphous system.

is enough to reduce the thermal conductivity of Si by almost a factor of 2.¹² In the case of the $Ni_{0.55}Pd_{0.45}$ alloy, the atomic species are chemically similar but both the mass disorder ($m_{Pd}/m_{Ni} \approx 2$) and concentration are large ($g = 0.078$) and good agreement is seen with the Eq. .¹³

While , the effect of explicit disorder has been demonstrated in the calculation of the intrinsic phonon lifetimes.⁵

Experimental measurements of isotopically pure and Ge-doped Si epitaxial layers demonstrate the original theory by Abeles can predict thermal conductivity in dilute alloys. Abeles also found good agreement with dilute predictions for both experimental measurements of both Si-Ge alloys and also (Ga,In)As alloys.¹¹ However, both of these alloy systems have a relatively high thermal conductivities (on the order of 1-10 W/m-K at 300 K). However, in the heavily disordered system In(As,P)

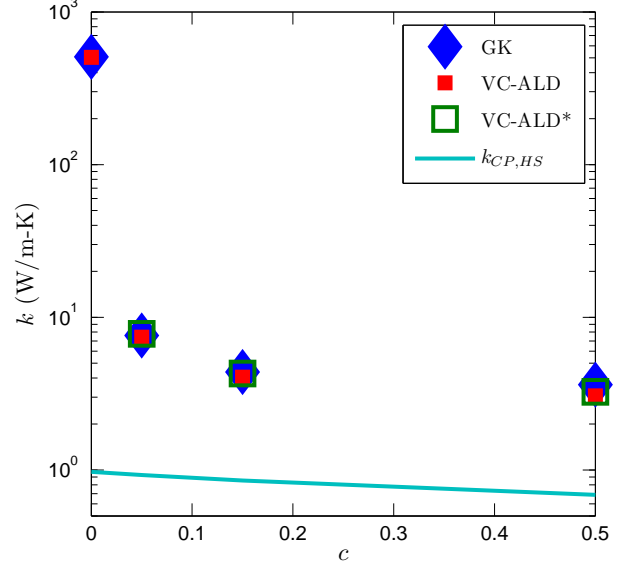


FIG. 10: The vibrational conductivity of LJ alloys predicted using MD simulations and the Green-Kubo method. The predicted thermal conductivities are for a LJ alloy of the form $m_{1-c}^a m_c^b$, where $m^a = 1$, $m^b = 3$, and $m_r = m^a/m^b = 3$ (in LJ units). As the alloy concentration is increased perturbatively, the vibrational conductivity drops quickly and saturates to a minimum at $c = 0.5$. For $c = 0.5$ the system is heavily disordered and the vibrational conductivity approaches that of an amorphous system.

(mass ratio of 3.7) worse agreement with the Abeles theory is observed.

The theory by Tamura is able to treat disorder scattering in an arbitrary crystal with dispersion. The theory, however, fails to predict the lifetimes of high-frequency modes, which are critical to the total thermal conductivity in LJ argon (see Fig. and). To match the predicted phonon lifetime at high frequency for $c = 0.05$ ($\tau(\kappa) \propto const.$, Fig.), the Tamura theory requires a DOS which scales as $D(\omega(\nu)) \propto const.$. Clearly from Fig. , this is not the case with either the VC or Gamma modes. To match the predicted phonon lifetime at high frequency for $c = 0.5$ ($\tau(\kappa) \propto 1/\omega(\nu)$, Fig. , also true for all c in SW silicon),

While Broido found that omission of optical scattering overpredicts the thermal conductivity of bulk Si by a factor of 2-3, optical modes contribute less than 5% to thermal conductivity itself. Similarly, the diffusivity adjusted thermal conductivities of SW Si are increased by less than 5%, demonstrating the unimportance of the high frequency “optical” modes in SW Si alloys.

the problem is with taud. VC-NMD agrees well with GK for both LJ and SW, while ALD-taud underpredicts for LJ. VC-NMD and ALD-taud use the same group velocity and classical specific heat.

Particularly challenging is predicting a representative

group velocity for modes in a disordered systems. Use of the VC approximation is a theoretically and computationally simple way to predict a representative group velocity.

High thermal conductivity materials tend to have a conductivity spectrum which is peaked in the low frequency range.(cite) It is in this range where the mode lifetimes follow closely the scalings with frequency which can be predicted by treating intrinsic and disorder scattering as perturbations (Eq.).

In contrast, in LJ argon the high frequency phonon mode properties are critical to the thermal transport.(cite) While the low frequency phonon properties predicted by VC-NMD and VC-ALD agree, it is the failure of the perturbative models at high frequency which causes VC-ALD to underpredict. The failure to account for harmonic disordered scattering due to the AF theory is responsible for causing both VC-NMD and VC-ALD to underpredict versus GK, which affects the high frequency modes significantly. LJ argon, with lower frequencies, lifetimes, and group velocities compared to “stiff” SW silicon, is considered a “soft” system. The predictions using VC-NMD, VC-ALD demonstrate the importance of explicit disorder modeling in “soft” systems and possible underprediction of the thermal properties.⁷

For SW silicon, the low frequency modes dominate thermal transport even in the heavily disordered alloy.(cite new Hopkins) It is thus unsurprising that predictions for SW silicon using VC-ALD agree well with VC-NMD and GK. This is also a plausible explanation for the success of predictions using VC-ALD and ab initio calculations compared to experiment for “stiff” systems (i.e. Si-Ge, GaN, and Diamond).(cite)

In SW silicon even the amorphous phase has significant contributions from propagating modes which can be considered to be phonons. This is can be seen by comparing the thermal conductivity predicted for the SW silicon amorphous phase ($k_{GK} = 3 \text{ W/m-K}$ (cite)) compared to $k_{CP,HS} = 0.5 \text{ W/m-K}$. For LJ argon in the amorphous phase, $k_{GK} = 0.121 \text{ W/m-K}$ and $k_{CP,HS} = 0.12 \text{ W/m-K}$, indicating that all important modes to thermal transport are non-propagating.

V. SUMMARY

Appendix A: Finite Simulation-Size Scaling for Thermal Conductivity

To predict a bulk thermal conductivity, extrapolation is used by the following finite size scaling $1/k \propto 1/N_0$. For VC-NMD and VC-ALD, the validity of this finite-size scaling is the low frequency modes in the finite system must be dominated by intrinsic scattering such that $\tau(\kappa) \propto \omega(\kappa)^{-2}$ and approximately follow the Debye approximation with respect to $v_{g,n}$ and DOS $D(\omega(\kappa))$.⁸ For LJ argon, this requirement is satisfied for modest system sizes (for $N_0 = 6$ to 12) so that both VC-NMD

and VC-ALD predictions can be extrapolated to a bulk value. For SW silicon, the thermal conductivity is dominated by low-frequency modes (Fig.). Becasue of this, large system sizes (up to $N_0 = 24$) are needed to satsify the extrpaolation requirements and only VC-ALD can be used.(cite) This underlines the computational effieney of the VC-ALD method which is necessary when computationally expensive ab initio methods are used (Section).^{4,5,7,44} For the GK method, the finite size extrapolation is used for both LJ argon and SW silicon for smaller system sizes $N_0 \leq 12$. The validity of this result can be explained in terms of a combination of effects which are specific to the MD simulations.⁴⁴ In fact, for $c = 0$ the GK results are independent of system size for $N_0 = 4$ to $N_0 = 12$ for both LJ argon and SW silicon.

- ^{*} Electronic address: mcgaughey@cmu.edu
- ¹ D. A. Broido, M. Maloney, G. Birner, N. Mingo, and D. Stewart, Applied Physics Letters **91**, 231922 (2007).
 - ² A. Ward, D. A. Broido, D. A. Stewart, and G. Deinzer, Phys. Rev. B **80**, 125203 (2009).
 - ³ A. Ward and D. A. Broido, Phys. Rev. B **81**, 085205 (2010), URL <http://link.aps.org/doi/10.1103/PhysRevB.81.085205>.
 - ⁴ L. Lindsay, D. A. Broido, and T. L. Reinecke, Phys. Rev. Lett. **109**, 095901 (2012), URL <http://link.aps.org/doi/10.1103/PhysRevLett.109.095901>.
 - ⁵ J. Garg, N. Bonini, B. Kozinsky, and N. Marzari, Phys. Rev. Lett. **106**, 045901 (2011), URL <http://link.aps.org/doi/10.1103/PhysRevLett.106.045901>.
 - ⁶ T. Shiga, J. Shiomi, J. Ma, O. Delaire, T. Radzynski, A. Lusakowski, K. Esfarjani, and G. Chen, Phys. Rev. B **85**, 155203 (2012), URL <http://link.aps.org/doi/10.1103/PhysRevB.85.155203>.
 - ⁷ Z. Tian, J. Garg, K. Esfarjani, T. Shiga, J. Shiomi, and G. Chen, Phys. Rev. B **85**, 184303 (2012), URL <http://link.aps.org/doi/10.1103/PhysRevB.85.184303>.
 - ⁸ J. Shiomi, K. Esfarjani, and G. Chen, Physical Review B **84**, 104302 (2011).
 - ⁹ N. d. Koker, Physical Review Letters **103**, 125902 (2009), URL <http://link.aps.org/abstract/PRL/v103/e125902>.
 - ¹⁰ H. Bao, B. Qiu, Y. Zhang, and X. Ruan, Journal of Quantitative Spectroscopy and Radiative Transfer **113**, 1683 (2012), ISSN 0022-4073, URL <http://www.sciencedirect.com/science/article/pii/S0022407312002336>.
 - ¹¹ B. Abeles, Phys. Rev. **131**, 19061911 (1963), URL <http://link.aps.org/doi/10.1103/PhysRev.131.1906>.
 - ¹² D. G. Cahill and F. Watanabe, Phys. Rev. B **70**, 235322 (2004), URL <http://link.aps.org/doi/10.1103/PhysRevB.70.235322>.
 - ¹³ W. A. Kamitakahara and B. N. Brockhouse, Phys. Rev. B **10**, 12001212 (1974), URL <http://link.aps.org/doi/10.1103/PhysRevB.10.1200>.
 - ¹⁴ K. Momma and F. Izumi, Journal of Applied Crystallography **41**, 653658 (2008), URL <http://dx.doi.org/10.1107/S0021889808012016>.
 - ¹⁵ J. M. Ziman, *Electrons and Phonons* (Oxford, New York, 2001).
 - ¹⁶ R. Peierls, *Quantum Theory of Solids* (Oxford University Press, 2001).
 - ¹⁷ D. A. McQuarrie, *Statistical Mechanics* (University Science Books, Sausalito, 2000).
 - ¹⁸ M. T. Dove, *Introduction to Lattice Dynamics* (Cambridge, Cambridge, 1993).
 - ¹⁹ J. V. Goicochea, M. Madrid, and C. H. Amon, Journal of Heat Transfer **132**, 012401 (2010).
 - ²⁰ D. P. Sellan, J. E. Turney, A. J. H. McGaughey, and C. H. Amon, Journal of Applied Physics **108**, 113524 (2010).
 - ²¹ J. D. Gale and A. L. Rohl, Molecular Simulation **29**, 291 (2003).
 - ²² A. M. Bouchard, R. Biswas, W. A. Kamitakahara, G. S. Grest, and C. M. Soukoulis, Phys. Rev. B **38**, 1049910506 (1988), URL <http://link.aps.org/doi/10.1103/PhysRevB.38.10499>.
 - ²³ J. C. Duda, T. S. English, D. A. Jordan, P. M. Norris, and W. A. Soffa, Journal of Physics: Condensed Matter **23**, 205401 (2011), URL <http://stacks.iop.org/0953-8984/23/i=20/a=205401>.
 - ²⁴ D. Donadio and G. Galli, Phys. Rev. Lett. **102**, 195901 (2009).
 - ²⁵ Y. He, D. Donadio, and G. Galli, Applied Physics Letters **98**, 144101 (2011).
 - ²⁶ Y. He, D. Donadio, J.-H. Lee, J. C. Grossman, and G. Galli, ACS Nano **5**, 1839{ }961844 (2011).
 - ²⁷ P. B. Allen, J. L. Feldman, J. Fabian, and F. Wooten, Philosophical Magazine B **79**, 1715 (1999).
 - ²⁸ S. N. Taraskin and S. R. Elliott, Philosophical Magazine Part B **79**, 17471754 (1999), URL <http://www.tandfonline.com/doi/abs/10.1080/13642819908223057>.
 - ²⁹ J. A. Thomas, J. E. Turney, R. M. Iutzi, C. H. Amon, and A. J. H. McGaughey, Physical Review B **81**, 081411(R) (2010).
 - ³⁰ Z.-Y. Ong, E. Pop, and J. Shiomi, Physical Review B **84**, 165418 (2011).
 - ³¹ B. Qiu, H. Bao, G. Zhang, Y. Wu, and X. Ruan, Computational Materials Science **53**, 278 (2012), ISSN 0927-0256, URL <http://www.sciencedirect.com/science/article/pii/S0927025611004770>.
 - ³² J. E. Turney, PhD thesis, Carnegie Mellon University, Pittsburgh, PA (2009).
 - ³³ D. J. Ecsedy and P. G. Klemens, Phys. Rev. B **15**, 59575962 (1977), URL <http://link.aps.org/doi/10.1103/PhysRevB.15.5957>.
 - ³⁴ S.-i. Tamura, Phys. Rev. B **27**, 858866 (1983), URL <http://link.aps.org/doi/10.1103/PhysRevB.27.858>.
 - ³⁵ P. G. Klemens, Proceedings of the Physical Society. Section A **68** (1955).
 - ³⁶ P. G. Klemens, Proceedings of the Physical Society. Section A **70**, 833 (1957), URL <http://stacks.iop.org/0370-1298/70/i=11/a=407>.
 - ³⁷ A. Skye and P. K. Schelling, Journal of Applied Physics **103**, 113524 (2008), URL <http://link.aip.org/link/?JAP/103/113524/1>.
 - ³⁸ P. B. Allen and J. L. Feldman, Physical Review B **48**, 1258112588 (1993).
 - ³⁹ D. Cahill and R. Pohl, Annual Review of Physical Chemistry **39**, 93121 (1988).
 - ⁴⁰ J. L. Feldman, M. D. Kluge, P. B. Allen, and F. Wooten, Physical Review B **48**, 1258912602 (1993).
 - ⁴¹ S. Shenogin, A. Bodapati, P. Kebelinski, and A. J. H. McGaughey, Journal of Applied Physics **105**, 034906 (2009), URL <http://link.aip.org/link/?JAP/105/034906/1>.
 - ⁴² J. C. Duda, T. S. English, D. A. Jordan, P. M. Norris, and W. A. Soffa, Journal of Heat Transfer **134**, 014501 (2012).
 - ⁴³ D. G. Cahill, F. Watanabe, A. Rockett, and C. B. Vining, Phys. Rev. B **71**, 235202 (2005), URL <http://link.aps.org/doi/10.1103/PhysRevB.71.235202>.
 - ⁴⁴ K. Esfarjani, G. Chen, and H. T. Stokes, Physical Review B **84**, 085204 (2011).